

# Single-layer metal nanolenses with tight foci in far-field

Piotr Wróbel · Tomasz J. Antosiewicz · Jacek Pniewski ·  
Tomasz Szoplik

Received: 15 January 2010 / Accepted: 3 December 2010 / Published online: 7 January 2011  
© The Author(s) 2011. This article is published with open access at Springerlink.com

**Abstract** In simulations we analyze performance of plasmonic nanolenses made of a single metal layer. We consider the nanolenses in two configurations. In the first, the nanolens is a free-standing silver layer with no hole on the optical axis and double-sided concentric corrugations. In the second, the nanolens has a set of slits instead of grooves. This necessitates integrating the annular metal elements with a dielectric matrix. We examine the following parameters of the nanolenses: film thickness, diameter of an on-axis stop, and lattice constant of slits or double-sided concentric grooves, as well as depth and width of grooves. Due to radially polarized illumination lenses have foci of full widths at half maxima (FWHMs) better than half a wavelength, though foci formed by propagating waves do not decrease beyond the diffraction limit. Due to proper geometry of slits or double-sided grooves lenses have focal lengths of the order of a few wavelengths. Transmission of light through lenses with double-sided narrow grooves reaches 30% while through ones with slits exceeds 80%.

## 1 Introduction

The idea of imaging by means of nanoscale plasmonic devices goes far beyond possibilities of refractive or diffractive microlenses and lenslet arrays made of optically trans-

parent media. Nanoscale devices for imaging comprise several nanotools such as flat or corrugated thin metal films [1] and metal-dielectric multilayers [e.g. 2] as well as optical probes for scanning near-field optical microscopes (SNOM) [1, 3]. The probes are of various kinds: pure metal, metallized dielectric with aperture or spectrally tunable apertureless dielectric-metal-dielectric [4]. Wide interest in plasmonic lenses has started a decade ago, when transverse resolution considerably better than the Abbe resolution limit was predicted [5] and experimentally proven [6, 7]. A lot of research was devoted to generation of surface plasmon-polariton (SPP) waves on circular and elliptical gratings milled in thin Ag layers and to focusing of plasmons on lens surfaces [8–10]. At the same time, ways of fabricating extremely smooth patterned metal layers for plasmonics were sought [11]. In a recent paper by Chen et al. [12], a plasmonic lens made of concentric silver rings with on-axis stop and illuminated with radially polarized light is experimentally proven to concentrate evanescent fields into a narrow needle. The needle results from propagation of generated plasmons toward the lens axis and their constructive interference, which results in strong enhancement of polaritons over the on-axis stop.

Previous work on optical properties of single-layer lenses with grooves or slits was focused on such properties, as transmission mechanism through a continuous layer [13], role of concentric grooves flanking an aperture [14, 15] and slit widths on transmission [16]. Diameters of focal spots in the far-field depend on the use of linearly [17, 18] or radially polarized [12, 19] illumination. Use of a central aperture is beneficial for generating collimated beams from incident, e.g. unpolarized light [14]. In the case of radially polarized light a negligible amount of energy is present at the axis. There is no need of a central hole as light coupling to SPPs and back to photons on the back side of the lenses occurs

P. Wróbel (✉) · J. Pniewski · T. Szoplik  
Faculty of Physics, University of Warsaw, Pasteura 7,  
02-093 Warszawa, Poland  
e-mail: [piotr.wrobel@igf.fuw.edu.pl](mailto:piotr.wrobel@igf.fuw.edu.pl)

T.J. Antosiewicz  
Interdisciplinary Centre for Mathematical and Computational  
Modelling, University of Warsaw, Pawiańskiego 5A,  
02-106 Warsaw, Poland

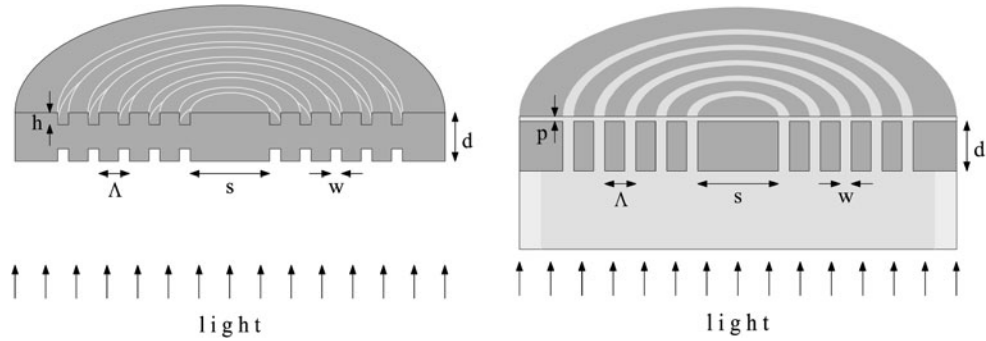


**Fig. 1** Schemes of a free-standing single Ag layer nanolens with double-sided concentric grooves (left) and nanolens made of concentric silver rings and integrated with a silica fiber and cladding. Thickness

of Ag layers is  $d$ , diameter of an on-axis stop is  $s$ , groove or slit lattice constant is  $\Lambda$  and groove or slit width is  $w$ . In a lens with grooves they are  $h$  deep, and in a lens with slits a dielectric cladding is  $p$  thick

away from the axis. Coupling between circular grooves or slits operating above the cut-off ensures optimum transmission.

In this paper we deal with plasmonic nanolenses in the form of a single metal layer either grooved and continuous [20] or with slits. We analyze focusing properties of such lenses in the far-field rather than their abilities to confine the SPP wave. As a consequence, we do not achieve superresolution, which is possible in the near-field due to contribution of evanescent fields.

## 2 Nanolenses and simulation tool

Figure 1 show schematic views of the two considered nanolenses. The left side shows a lens in the form of a free-standing silver nanolayer with concentric corrugations on both surfaces and no hole at the optical axis [20]. On the right, a lens is composed of annular Ag rings and an on-axis stop which are integrated with an optical fiber and dielectric antioxidation cladding. A silver film of thickness  $d$  is deposited onto a flat end of a multimode silica fiber of core diameter  $2r = 10 \mu\text{m}$  with permittivity values  $\varepsilon_c = 2.12$  and  $\varepsilon_l = 2.11$  of core and cladding, respectively. Periodic slits of width  $w$  and lattice constant  $\Lambda$  are filled with the same dielectric as that of the fiber core. Transmission of light through the lenses of both types is conditioned by efficient photon-plasmon and plasmon-photon coupling, where momentum matching is ensured due to the groove/slit periodicity  $\Lambda - w = 2\lambda_{\text{SPP}}$ , where  $\lambda_{\text{SPP}}$  is the SPP wavelength. The grating coupling method makes use of the reciprocal vector of the grating  $k_g = 2\pi/\Lambda$ , which shifts the wavevector of impinging light to the value of the wavevector of the SPP wave  $k_{\text{SPP}}$

$$k_{\text{SPP}} = k_0 n \sin \varphi + q k_g, \quad (1)$$

where  $k_0$  is the wavevector in free space,  $\varphi$  is the angle of incidence,  $n$  is the refractive index of air (left side lens) or glass (right), and  $q$  is an integer.

Photon-plasmon momentum matching is efficient on the whole perimeters of grooves or slits due to radially polarized illumination with Laguerre–Gauss (LG) intensity profile [19, 20]. The axis of symmetry of grooves and slits coincides with the optical axis of the incident LG beam with pure radial polarization and radial beam profile of electric field

$$E_r(r) = \left( \frac{r}{R} \right) \exp \left( -\frac{r^2}{2R^2} \right), \quad (2)$$

where  $R$  is a radius of maximum intensity. Matching the beam diameter with that of grooved or perforated areas maximizes efficient use of light energy, that is, we have efficient photon-plasmon coupling on outer edges of grooves or slits. Each point of these edges on the backside of the lenses radiates spherical waves, which contribute to the focus.

Simulations are performed in cylindrical coordinates with the finite-difference time domain (FDTD) method using freeware package Meep [21] and in-house body-of-revolution FDTD code [4, 20]. Silver is modeled using Drude dispersion  $\varepsilon(\omega) = \varepsilon_\infty - \omega_p^2/[\omega(\omega + i\Gamma)]$  with the following parameters  $\varepsilon_\infty = 3.70$ ,  $\omega_p = 13673 \text{ THz}$  and  $\Gamma = 27.35 \text{ THz}$  [4, 20, 22]. We use a Cartesian grid of spatial discretization 2 nm. Transmission properties are analyzed for the following ranges of lens parameters: silver layer thickness  $d$  from 80 to 500 nm, slit width  $w$  from 20 to 400 nm, lattice constant  $\Lambda$  from 400 to 800 nm, and groove depth  $h$  from 10 to 40 nm. Other parameters are kept constant: the dielectric cladding thickness  $p = 10 \text{ nm}$ , the fiber-core radius  $r = 5 \mu\text{m}$ , and, dependent on  $r$ , the radius of maximum beam intensity  $R = 1.7 \mu\text{m}$ .

## 3 Transmission of nanolenses

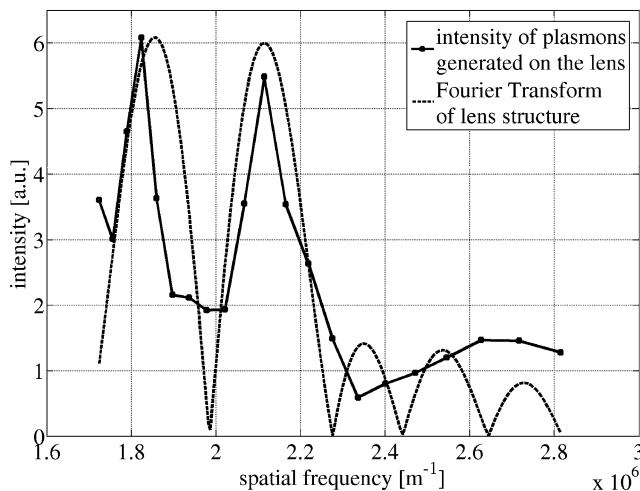
Figure 2 shows intensity distributions of plasmons generated on the backside of a grooved lens, shown with a solid line with squares, and the Fourier Transform (FT) of the structure geometry of exactly the same lens, shown with a dashed

line, as a function of the plasmon and structure spatial frequency. According to (1), the frequency matching condition is, in our case of  $\varphi = 0$ , entirely dependent on the values of  $k_g$  provided by the profile of the lenses. Thus, relative intensities of generated SPP waves with spatial frequencies  $k_{\text{SPP}}/2\pi$  are dependent on  $k_g$  and are the higher the greater is  $k_g$  intensity in FT of the lens profile. We theoretically predict that incident light in the wavelength range  $\lambda$  of 400 to 800 nm couples most efficiently to SPP waves for  $1/\lambda_{\text{SPP}} = 1.86 \times 10^6 \text{ m}^{-1}$  (which corresponds to  $\lambda_0 \approx 560 \text{ nm}$  in free space) and  $1/\lambda_{\text{SPP}} = 2.11 \times 10^6 \text{ m}^{-1}$  ( $\lambda_0 \approx 500 \text{ nm}$ ) and with smaller efficiency for spatial frequencies greater than  $2.3 \times 10^6 \text{ m}^{-1}$ . This is confirmed by an analysis of SPP wave intensity on the backside of the lens, where we observe maxima at  $1/\lambda_{\text{SPP}} = 1.75 \times 10^6 \text{ m}^{-1}$  ( $\lambda_0 \approx 570 \text{ nm}$ ) and  $1/\lambda_{\text{SPP}} = 1.86 \times 10^6 \text{ m}^{-1}$  ( $\lambda_0 \approx 500 \text{ nm}$ ).

Once photons are coupled to plasmons on the input sides of the lenses different mechanisms govern transition of elec-

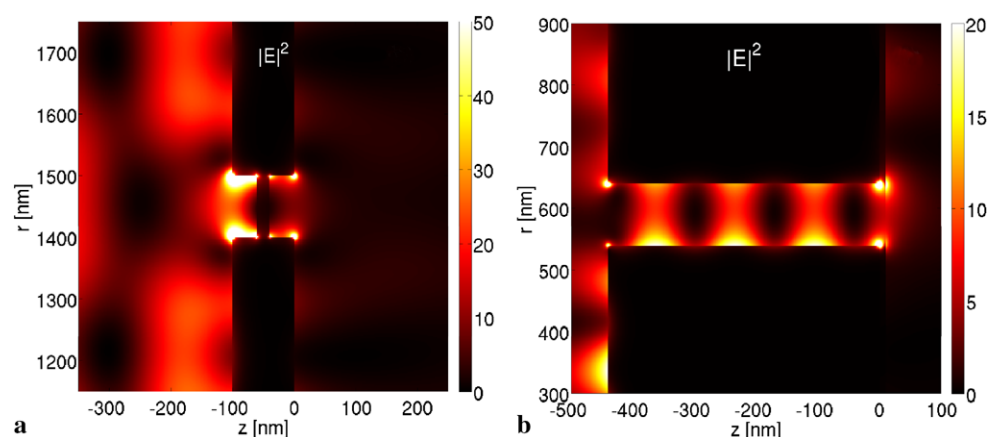
tron oscillations to the output sides, depending on whether grooves or slits are present. In the lens with double-sided grooves transmission of light results from resonant tunneling via strongly localized surface plasmons in a manner recognized in an early paper of Tan et al. [23]. This coupling of plasmons from grooves on the incident surface to ones in grooves on the back surface is shown in Fig. 3a. Transmission through this nanolens, based on resonant tunneling, reaches 30%. In the case of a lens with slits, increased transmission results from coupling light directly to waveguided modes in the slits. It can be further enhanced by properly tuning the thickness of the metal film to exploit Fabry–Pérot resonances of guided SPP modes in narrow channels [24, 25], as seen in Fig. 3b. Transmission of light through the second nanolens, dependent on guided modes, approaches 80%.

The large difference in transmittance of the considered lenses is a result of their structure. For the nanolens with grooves transmission results from coupling plasmons across a 20 nm silver layer. Guided modes in concentric slits are the transmission mechanism of the second lens. For the analyzed spectrum they operate above cut-off and have a large transmission even for small widths.



**Fig. 2** Intensity (in arbitrary units) of plasmons generated on the backside of a grooved lens (solid line with squares) and the FT of the structure of the same lens (dashed line) as a function of the plasmon and structure spatial frequency

**Fig. 3** Electric energy density distributions in (a) grooves for wavelength  $\lambda = 400 \text{ nm}$  and in (b) slits for  $\lambda = 500 \text{ nm}$ . (a) Localized plasmons in grooves on the incident side couple via resonant tunneling to plasmons on the other side of metal links. (b) In slits energy is transported by waveguided SPP modes, which show Fabry–Pérot resonances



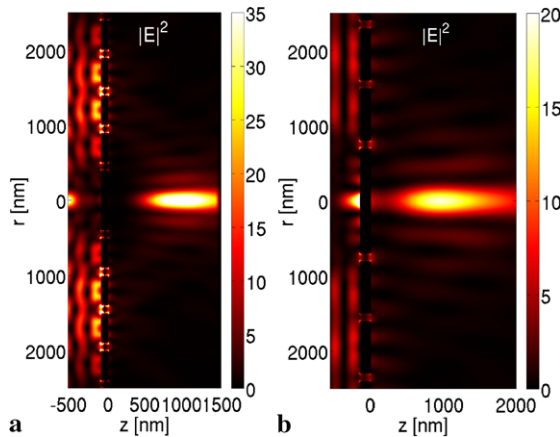


**Fig. 4** Electric energy density in the vicinity of simulated nanolenses (a) with grooves for wavelength  $\lambda = 400$  nm and (b) with slits for  $\lambda = 700$  nm

radiative nature and propagate into the far-field, where they contribute to focusing in such a way that the radial electric field component interferes destructively at the axis and its energy flows into the longitudinal component. Because this constructive interference takes place in the far-field, where evanescent components will have decayed, the transversal dimensions of the focal spots are limited by diffraction. In both cases the mechanism of focus formation is similar to that in classical refractive optics, though very different from that in diffractive optical elements. Foci formed by these lenses have FWHMs slightly bigger than  $0.4\lambda$  and their focal lengths depend on the wavelength of incident light and range from one to a few  $\lambda$ . Both nanolenses focus LG beams as tightly as classical high-NA refractive optical systems. Figure 4 shows electric energy densities in focal regions of both lenses. A characteristic separation of foci from the metal surface can be seen, which is very different from plasmonic needles observed in other works [12].

## 5 Conclusions

A free-standing 3D silver nanolens with concentric double-sided grooves and no hole on the optical axis is illuminated with a radially polarized visible range Laguerre-Gauss beam. The second nanolens is composed of annular Ag rings and an on-axis stop which are integrated with an optical fiber and a dielectric antioxidation cladding. Both lenses focus light in the far-field into spots of FWHM conforming to the diffraction limit. Their focal lengths depend on wavelength and range from one to a few  $\lambda$ . In both cases foci are formed in a similar way. Behind the lenses radial components of transmitted electric field scatter on backside edges of grooves or slits, propagate and interfere destructively on the axis. The longitudinal component of transmitt-

ted electric field, in turn, interferes constructively. Transmission through the continuous nanolens with grooves is based on resonant tunneling and for resonant frequencies reaches 30%. Transmission of light through the nanolens composed of rings embedded in a dielectric matrix results from coupling light to waveguided modes in the slits and reaches 80%. Both nanolenses concentrate radially polarized LG illumination as tightly as classical high-NA refractive optical systems. The proposed nanolenses may be employed for nanolithography [26] and endoscopy [27].

**Acknowledgements** This work has been supported by the Polish Ministry of Science and Higher Education under the project N N507 445534 and the National Centre for R&D under the project N R15 0018 06. The authors are partners in COST Actions MP 0702 and MP 0803. Numerical computations were performed in the Interdisciplinary Centre for Mathematical and Computational Modelling (ICM), University of Warsaw, grant number G33-7.

**Open Access** This article is distributed under the terms of the Creative Commons Attribution Noncommercial License which permits any noncommercial use, distribution, and reproduction in any medium, provided the original author(s) and source are credited.

## References

1. S. Kawata, Y. Inouye, P. Verma, Nat. Photonics **3**, 388 (2009)
2. R. Kotynski, T. Stefaniuk, J. Opt. A, Pure Appl. Opt. **11**, 015001 (2009)
3. L. Novotny, B. Hecht, *Principles of Nano-Optics* (Cambridge University Press, Cambridge, 2007)
4. T.J. Antosiewicz, P. Wróbel, T. Szoplik, Opt. Express **17**, 9191 (2009)
5. J.B. Pendry, Phys. Rev. Lett. **85**, 3966 (2000)
6. D.O.S. Melville, R.J. Blaikie, C.R. Wolf, Appl. Phys. Lett. **84**, 4403 (2004)
7. N. Fang, H. Lee, C. Sun, X. Zhang, Science **308**, 534 (2005)
8. Z. Liu, J.M. Steele, W. Srituravanich, Y. Pikus, C. Sun, X. Zhang, Nano Lett. **5**, 1726 (2005)
9. C.K. Chang, D.Z. Lin, C.S. Yeh, C.K. Lee, Y.C. Chang, M.W. Lin, J.T. Yeh, J.M. Liu, Appl. Phys. Lett. **90**, 061113 (2007)
10. W. Srituravanich, L. Pan, Y. Wang, C. Sun, D.B. Bogy, X. Zhang, Nat. Nanotechnol. **3**, 733 (2008)
11. P. Nagpal, N.C. Lindquist, S.H. Oh, D.J. Norris, Science **325**, 594 (2009)
12. W. Chen, D.C. Abeyasinghe, R.L. Nelson, Q. Zhan, Nano Lett. **9**, 4320 (2009)
13. N. Bonod, S. Enoch, L. Li, E. Popov, M. Neviere, Opt. Express **11**, 482 (2003)
14. H.J. Lezec, A. Degiron, E. Devaux, R.A. Linke, L. Martin-Moreno, F.J. Garcia-Vidal, T.W. Ebbesen, Science **297**, 820 (2002)
15. F.I. Baida, D. Van Labeke, B. Guizal, Appl. Opt. **42**, 6811 (2003)
16. H. Shi, C. Wang, C. Du, X. Luo, X. Dong, H. Gao, Opt. Express **13**, 6815 (2005)
17. D.Z. Lin, C.H. Chen, C.K. Chang, T.D. Cheng, C.S. Yeh, C.K. Lee, Appl. Phys. Lett. **92**, 233106 (2008)
18. J. Wang, J. Zhang, X. Wu, H. Luo, Q. Gong, Appl. Phys. Lett. **94**, 081116 (2009)
19. Q. Zhan, Adv. Opt. Photon. **1**, 1 (2009)
20. P. Wróbel, J. Pniewski, T.J. Antosiewicz, T. Szoplik, Phys. Rev. Lett. **102**, 183902 (2009)

21. A.F. Oskooi, D. Roundy, M. Ibanescu, P. Bermel, J.D. Joannopoulos, S.G. Johnson, *Comput. Phys. Commun.* **181**, 687 (2010)
22. T.J. Antosiewicz, T. Szoplik, *Opt. Express* **15**, 7845 (2007)
23. W.C. Tan, T.W. Preist, R.J. Sambles, *Phys. Rev. B* **62**, 11134 (2000)
24. J.A. Porto, F.J. Garcia-Vidal, J.B. Pendry, *Phys. Rev. Lett.* **83**, 2845 (1999)
25. S. Astilean, Ph. Lalanne, M. Palamaru, *Opt. Commun.* **175**, 265 (2000)
26. Y. Wang, W. Srituravanich, C. Sun, X. Zhang, *Nano Lett.* **8**, 3041 (2008)
27. R.A. Natalin, J. Landman, *Nat. Rev. Urol.* **6**, 622 (2009)